

Surface-Regulated Platinum–Copper Nanoframes in Electrochemical Reforming of Ethanol for Efficient Hydrogen Production

Hui Fu, Nan Zhang,* Feili Lai, Longsheng Zhang, Suli Chen, Hanjun Li, Kezhu Jiang, Ting Zhu, Fangping Xu, and Tianxi Liu*



Cite This: *ACS Catal.* 2022, 12, 11402–11411



Read Online

ACCESS |

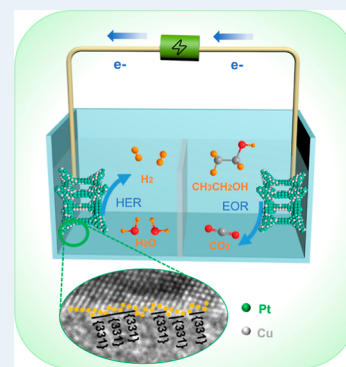
Metrics & More

Article Recommendations

Supporting Information

ABSTRACT: Replacing the kinetics sluggish oxygen evolution reaction with thermodynamically favorable ethanol oxidation reaction (EOR) is a prospective method to boost energy-efficient hydrogen production. Surface regulation has achieved great success in enhancing catalytic performance, but it has been rarely demonstrated for the coupled hydrogen evolution reaction (HER)/EOR to date. Herein, the three-dimensional PtCu nanoframe (NF) with high-index facets and multi-channels is designed through a dealloying strategy to achieve bifunctional catalysis for HER and EOR. The PtCu NF/C needs only 0.58 V to arrive at 10 mA cm⁻² in the coupled HER/EOR, while 1.88 V is required in water splitting. Moreover, ethanol can be oxidized by PtCu NF/C to acetate with a high Faradaic efficiency of 92%. Mechanistic studies reveal that the combination of the three-dimensional structure, Cu introduction, and high-index facets endows the PtCu NF/C with enhanced adsorption capacity for ethanol and H₂O, as well as dissociation capacity for C–H bonds of ethanol. This work is the icing on the cake for bifunctional electrocatalysts and the further development of energy-saving hydrogen evolution.

KEYWORDS: PtCu nanoframes, high-index facets, multi-channel structure, hydrogen evolution reaction, ethanol oxidation reaction



INTRODUCTION

Electrolysis of water, an environmentally friendly and prospective technique to produce high purity hydrogen (H₂) with zero-carbon, has received extensive attention.^{1–3} Nevertheless, the kinetics sluggish oxygen evolution reaction (OER) has seriously hampered the conversion efficiency of water electrolysis.^{4–6} Although advanced bifunctional electrocatalysts have been developed to facilitate hydrogen evolution reaction (HER) and OER, the needed voltage for overall water splitting still maintains 1.6–2.0 V.^{7,8} Lately, combining ethanol oxidation reaction (EOR) with HER to produce valuable chemicals and H₂ is a promising approach due to its high energy density, low toxicity, and valuable upgrading by-product.⁹

To accelerate the development of this emerging field, more attention should be paid to designing efficient bifunctional electrocatalysts for HER and EOR. Some platinum (Pt)-based materials have showed excellent performance in HER and small molecule oxidation reactions, demonstrating their amazing properties in this realm.^{10–13} However, the performance and practical application of Pt are subjected to its high cost, weak adsorption capacity for ethanol and H₂O molecules, as well as the weak dissociation capacity for C–H bonds in ethanol, resulting in poor selectivity to ethanol-selective oxidation products, and so forth.¹⁴ Introducing foreign elements to form Pt-based alloy materials could enhance

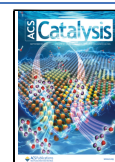
electron conductivity, optimize the electron structure, and provide sufficient synergistic function of the material. In addition, a three-dimensional (3D) open structure with multi-channels could not only expose enough active sites and improve utilization of Pt but also limit the reactants in nanoscale spaces to increase the collision frequency during the catalytic reaction process.^{15–20} The high-index facets are considered to be an open structure represented by a set of Miller indices $\{hkl\}$, which have rich low coordination atoms, providing more active sites for the catalytic process.^{21–23} However, the reported performance of bifunctional catalysts for HER and EOR is still unsatisfactory. Therefore, it is challenging and significant to develop Pt-based alloy electrocatalysts with 3D open structures and high-index facets for superior bifunctional performance (HER and EOR).

Herein, we designed a class of unique PtCu nanoframes (NFs) with high-index facets and multi-channels through a facile dealloying strategy for HER and EOR. The pristine solid PtCu nanodendrites (NDs) were initially synthesized (Figure

Received: June 23, 2022

Revised: August 16, 2022

Published: September 5, 2022



Scheme 1. Schematic Diagram for the Synthesis of PtCu NF

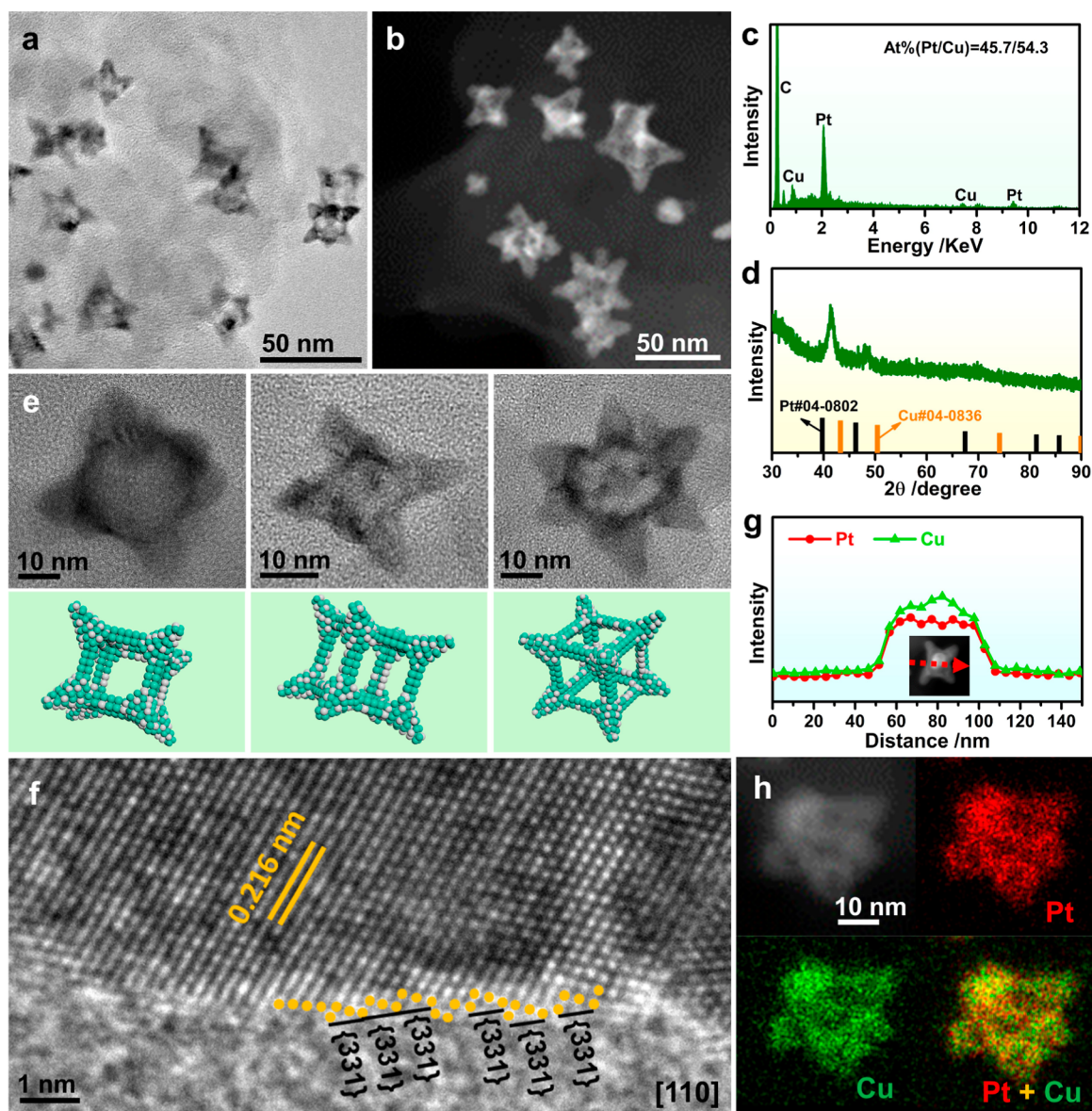
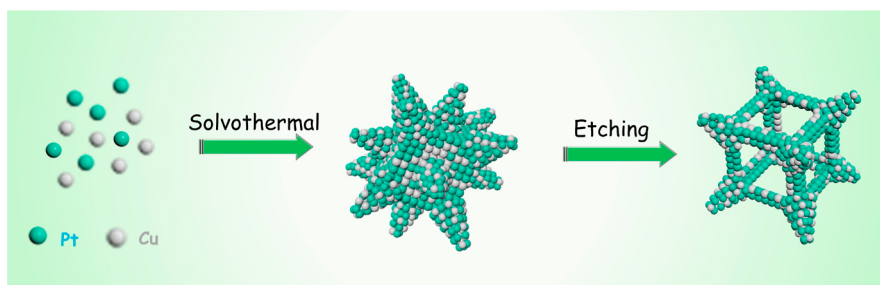


Figure 1. (a) TEM image, (b) HAADF-STEM image, (c) SEM-EDS spectrum, (d) PXRD pattern, (e) TEM images and schematic models of an individual PtCu NF viewed along with different angles, (f) HRTEM image, and (g) line-scanning of PtCu NF. The inset is the analyzed particle. (h) HAADF-STEM image and EDS elemental mappings of PtCu NF/C.

S1). Subsequently, the PtCu NF with high-index facets and multi-channels was obtained, after which Cu was selectively leached away by the acetic acid treatment (Scheme 1). The unique structure endows PtCu NF/C with abundant unsaturated sites and large surface area, which are highly favorable to provide more active sites for HER and EOR.

Specifically, PtCu NF/C exhibits excellent HER performance in alkaline and acidic electrolytes. In addition, PtCu NF/C also presents a lower oxidation potential and higher activity than PtCu ND/C and the commercial Pt/C in EOR. Furthermore, a two-electrode cell was fabricated by employing PtCu NF/C as a bifunctional electrocatalyst for HER and EOR. The two-

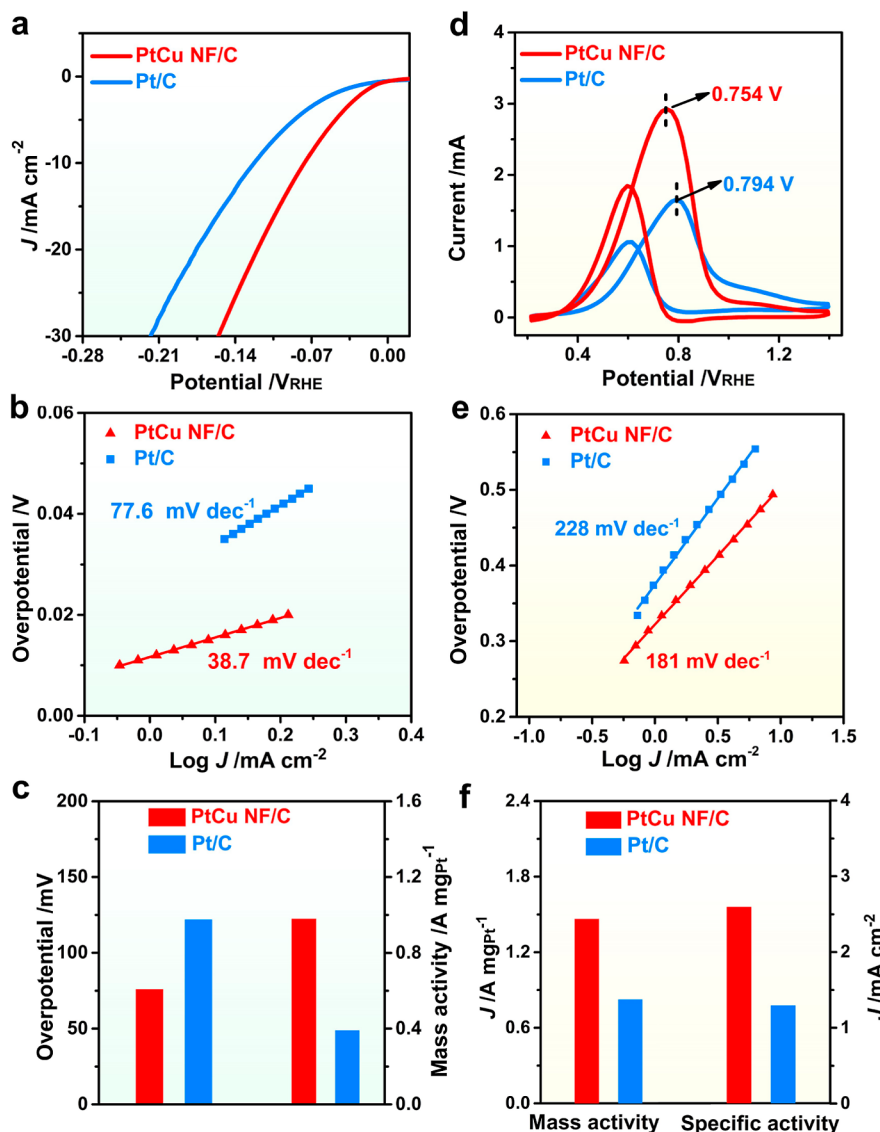


Figure 2. (a) LSV curves of PtCu NF/C and the commercial Pt/C in 1.0 M KOH. (b) Tafel plots and (c) overpotentials at 10 mA cm⁻² and mass activities at 76 mV_{RHE} of PtCu NF/C and the commercial Pt/C for HER. (d) CV curves, (e) Tafel plots, and (f) mass and specific activities of PtCu NF/C and the commercial Pt/C for EOR.

electrode cell needed only 0.58 V to achieve 10 mA cm⁻², which is much lower than 1.88 V for water splitting and the minimum theoretical value of the whole water splitting (1.23 V), outperforming PtCu ND/C and the commercial Pt/C. Last but not least, an efficient biomass conversion (ethanol of acetate) of 98.2% is obtained by PtCu NF/C, which is better than those of PtCu ND/C (48.6%) and commercial Pt/C (5.75%). Moreover, when ethanol was replaced with other alcohols (methanol, ethylene glycol, and glycerol), PtCu NF/C could also achieve energy-saving hydrogen production in the coupled HER/alcohol oxidation reaction.

RESULTS AND DISCUSSION

To obtain the PtCu NF/C, PtCu ND/C (Figure S2) was treated with acetic acid. It can be seen from X-ray photoelectron spectroscopy (XPS) analysis that Pt is in the metallic state, while Cu is in the oxidized state for PtCu ND/C (Figure S3). Furthermore, it is difficult to avoid the presence of a small amount of dissolved oxygen in acetic acid, and oxygen can easily further oxidize Cu to CuO. Acetic acid would react

with CuO through neutralization reaction to dissolve Cu into Cu²⁺. In addition, the chemical etching was carried out in acetic acid at 60 °C, further accelerating the oxidation of Cu and the etching process.^{24,25} Transmission electron microscopy (TEM) and high-angle annular dark-field scanning TEM (HAADF-STEM) images of the sample after the acid treatment shown in Figure 1a,b demonstrate that the initial PtCu ND/C catalysts have been successfully eroded into highly open structure. The multi-channel feature of PtCu NF/C is attributed to the sharp loss of the Cu component revealed in scanning electron microscopy–energy-dispersive X-ray spectroscopy (SEM–EDS) and inductively coupled plasma optical emission spectrometry (ICP–OES) (Figure 1c and Table S1). In addition, the powder X-ray diffraction (PXRD) pattern shows that the obtained PtCu NF/C is also the Pt–Cu alloy phase (Figure 1d), while the peaks slightly shift to lower angles than those of PtCu NDs due to the expanded *d*-spacing after the Cu has been etched. To clarify the structure and determine the specific morphology of PtCu NF/C, magnified images focused on an individual nanoparticle were further

captured at various angles (Figure 1e). The TEM images of the PtCu NF at different angles correspond well to the projections of the models, confirming the growth of NDs on the four vertices of the cubic NF. The high-resolution TEM (HRTEM) image obtained from a single PtCu NF indicates the interplanar spacing of 0.216 nm, which could be assigned to the {111} facet of PtCu alloy (Figure 1f). It can be found here that the lattice spacing becomes larger after the etching of Cu from PtCu NDs, which further corresponds to the positions of peaks in the PXRD pattern shifting to smaller values. What is more, plentiful high-index facets of {331} on the PtCu NF surface can be observed (Figure 1f), providing more active sites for catalysis.²⁶ Moreover, the line scan analysis reveals that the Cu and Pt distribute uniformly within the whole particle (Figure 1g), which is in line with the result of EDS elemental mappings (Figure 1h).

In order to further study the formation process of PtCu NF with multi-channels, we collected samples with different reaction times to characterize the structure and composition (Figures S4 and S5). We can see that the PtCu NDs with the multi-branched structure are the main products at the initial stage (Figure S4a). When the etching reaction proceeds to 0.5 h, the multi-branched structures changed to octapods with the dissolution of Cu and migration of Pt (Figures S4b and S5).²⁷ As the reaction proceeds (1–2 h), the Cu inside the octapods dissolves and gradually becomes a porous structure (Figure S4c,d). After 3 h of etching, the frame structure gradually emerges (Figure S4e), and the structures could remain stable until the reaction time reaches 5 h (Figure S4f). It can also be found from the PXRD patterns that the position of the main peak shifts to the lower angle as the reaction proceeds (Figure S4g). Particularly, after the reaction proceeded for 0.5 h, the diffraction peak shifts slightly to the low angle, and when the reaction proceeded for 1 h, the peak position changes significantly (Figure S4h). The composition of the intermediates measured by SEM–EDS reveals that at the beginning, a large amount of Cu was dissolved, and the compositions of the samples tend to be stable after 2 h (Figures S4i and S5). Above all, the formation of PtCu NF/C involves the structure evolution from PtCu octapods, porous octapods to NF with the dissolution of Cu and migration of Pt (Figure S4j).

The electrocatalytic performance of PtCu NF/C was investigated in a three-electrode system. The commercial Pt/C (HiSPEC 3000, Johnson Matthey, Figure S6) was taken as a reference for comparison. The loading amount of Pt in PtCu NF/C was fixed to 20 wt % by ICP–OES. The electrochemical specific surface areas (ECSAs) of PtCu NF/C and the commercial Pt/C were obtained by the hydrogen adsorption curves (Figure S7).²⁸ The ECSAs of PtCu NF/C and the commercial Pt/C were 56.27 and 61.42 m² g⁻¹, respectively. Initially, HER properties of the PtCu NF/C and the commercial Pt/C were investigated in 1.0 M KOH, before which, all the reference electrode potentials were calibrated to the reversible hydrogen electrode (Figure S8). Figure 2a compares the linear sweep voltammetry (LSV) curves of PtCu NF/C and the commercial Pt/C, among which the PtCu NF/C possesses an exceptional electrocatalytic activity for HER. The corresponding Tafel slope of the PtCu NF/C is 38.7 mV dec⁻¹, which is lower than that of the commercial Pt/C (77.6 mV dec⁻¹), suggesting the favorable reaction kinetics of PtCu NF/C (Figure 2b).²⁹ As shown in Figure 2c, PtCu NF/C exhibits an overpotential of 76 mV at 10 mA cm⁻², while 122

mV is required for the commercial Pt/C. In addition, compared with the 0.39 A mg_{Pt}⁻¹ of mass activity for the commercial Pt/C at 10 mA cm⁻², the mass activity for PtCu NF/C was calculated to be as high as 0.98 A mg_{Pt}⁻¹. In addition, the turnover frequency (TOF) values of PtCu NF/C in 1 M KOH were calculated by the estimated number of active sites. The TOF values of PtCu NF/C were 2.20 and 6.27 H₂ s⁻¹ at 50 and 100 mV, respectively, which are larger than those of PtCu ND/C (1.86 and 4.74 H₂ s⁻¹) and the commercial Pt/C (0.77 and 2.55 H₂ s⁻¹). In addition, after 10 h of electrolysis, PtCu NF/C exhibits the smaller reduction in overpotential than that of the commercial Pt/C, revealing their better catalytic stability for HER (Figure S9a). Furthermore, the electrochemical impedance spectroscopy (EIS) responses of PtCu NF/C and the commercial Pt/C were also investigated to evaluate the performance (Figure S9b). It is obvious that the PtCu NF/C has the smaller semicircle radius, corresponding to the lower charge-transfer resistance, resulting in the higher charge-transfer rate and faster catalytic kinetics than the commercial Pt/C.^{12,30–32}

Furthermore, the HER properties of PtCu NF/C and the commercial Pt/C were further investigated in 0.5 M H₂SO₄ (Figure S10). PtCu NF/C and the commercial Pt/C present the overpotentials of 14 and 32 mV at 10 mA cm⁻², respectively (Figure S10a). Moreover, PtCu NF/C exhibits the mass activity of 0.98 A mg_{Pt}⁻¹ at 10 mA cm⁻², which is about 1.4 times higher than that of the commercial Pt/C (0.7 A mg_{Pt}⁻¹) (Figure S10b). All the results show that PtCu NF/C possesses outstanding HER performance in a wide range of pH, outperforming the commercial Pt/C. The HER performances of PtCu ND/C were further studied. As shown in Figure S11, the PtCu NF/C also shows HER activity superior to the initial PtCu ND/C (overpotential of 92 mV and mass activity of 0.75 A mg_{Pt}⁻¹ in 1.0 M KOH, and overpotential of 28 mV and mass activity of 0.13 A mg_{Pt}⁻¹ in 0.5 M H₂SO₄).

In addition, PtCu nanocube frames (NCF)/C with low-index facets were prepared to evaluate the effect of surface regulation on the performance for HER (Figure S12). PtCu NCF/C shows the overpotentials of 88 and 17 mV, as well as 0.83 and 0.70 A mg_{Pt}⁻¹ of mass activity in 1.0 M KOH and 0.5 M H₂SO₄ (Figure S13), which are slightly inferior to those of the PtCu NF/C, indicating that the synergistic effect between the multi-channels and surface regulation of PtCu NF play the key role in enhancing the HER performance. Moreover, the excellent HER performance of PtCu NF/C overwhelmingly surpasses the most recently reported electrocatalysts (Table S2).

The EOR performance of PtCu NF/C and the commercial Pt/C was further investigated in 1.0 M KOH + 0.5 M ethanol. As shown in Figure 2d, the ethanol oxidation potential of the PtCu NF/C (0.754 V) is much lower than 0.794 V for the commercial Pt/C, revealing the enhanced ability to cleave C–H bonds of C₂H₅OH by PtCu NF/C.³³ The corresponding Tafel slopes of PtCu NF/C and the commercial Pt/C in EOR were 181 and 228 mV dec⁻¹ (Figure 2e), respectively, which indicates that the ethanol oxidation rate and reaction kinetics of PtCu NF/C are significantly improved. As shown in Figure 2f, the mass activities of PtCu NF/C and the commercial Pt/C are 1.5 and 0.8 A mg_{Pt}⁻¹, respectively. Furthermore, PtCu NF/C shows the specific activity of 2.6 mA cm⁻², while the specific activity of the commercial Pt/C is 1.3 mA cm⁻². After the *I*–*t* test (Figure S9c), the EOR current of PtCu NF/C has a lower decay rate compared with the commercial Pt/C, confirming

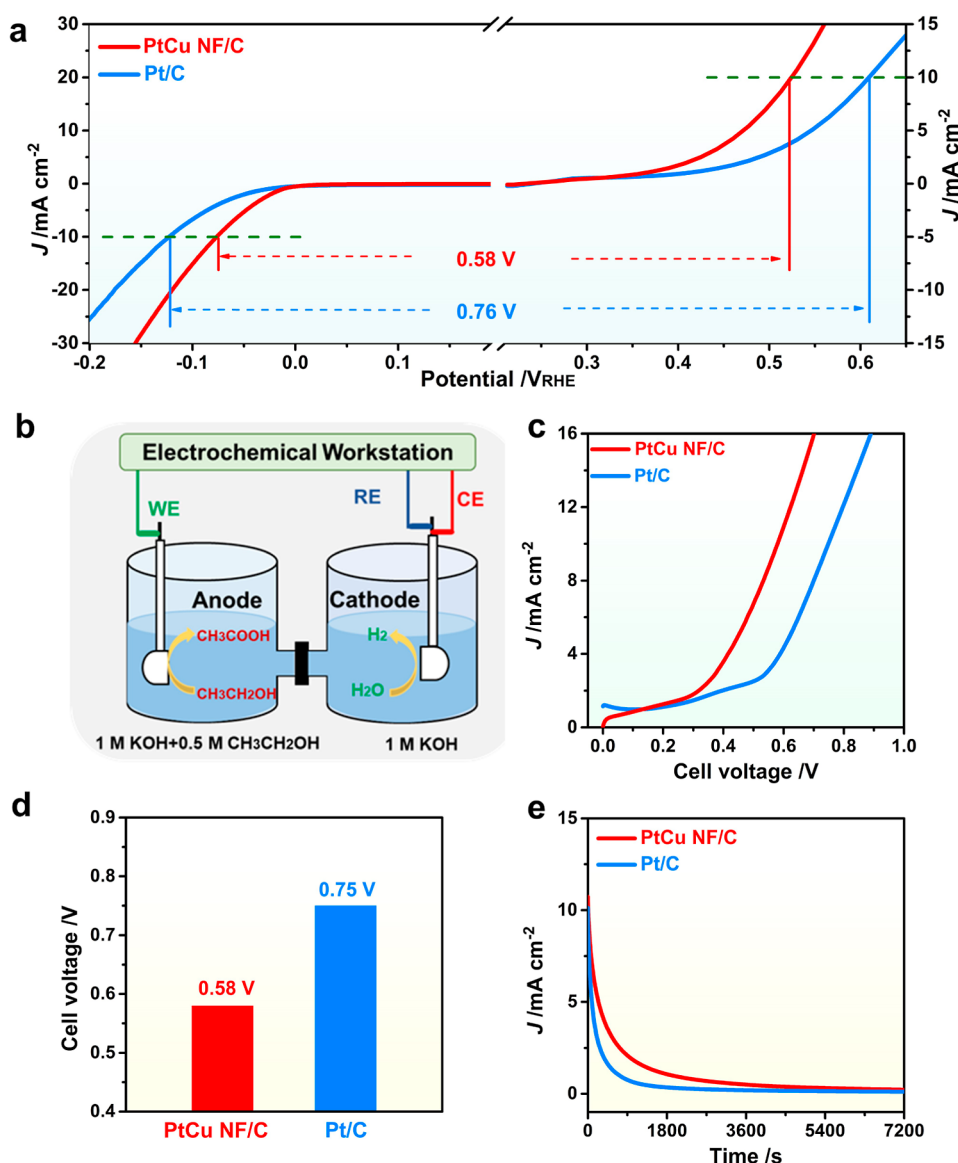


Figure 3. (a) Values of ΔE calculated from the HER and EOR polarization curves of catalysts in basic conditions. (b) Schematic of the two-electrode cell electrolyzer. (c) LSV curves for the coupled HER/EOR in the two-electrode cell electrolyzer. (d) Voltages needed at 10 mA cm^{-2} and (e) $I-t$ curves for the catalysts in HER/EOR.

the enhanced durability of PtCu NF/C for EOR. Moreover, the EOR activity of PtCu NF/C also outperforms the PtCu ND/C and PtCu NCF/C (1.3 and $1.3 \text{ A mg}_{\text{Pt}}^{-1}$ of mass activity, and 2.3 and 2.4 mA cm^{-2} of specific activity) (Figures S14 and S15), outperforming most of the reported electrocatalysts (Table S3) and further demonstrating the significant role of surface and structure regulation for the PtCu NF/C in EOR.

The products in the electrolyte obtained after 10 h of electrolysis at -0.78 V by PtCu NF/C, PtCu ND/C, and the commercial Pt/C were further analyzed by ^1H nuclear magnetic resonance ($^1\text{H NMR}$). Interestingly, as shown in Figure S16a–c, only acetate can be detected in the anodic electrolyte by PtCu NF/C, PtCu ND/C, and commercial Pt/C. Moreover, the yield of acetate produced by the three different catalysts at this potential was calculated by $^1\text{H NMR}$ (Figure S16d). Significantly, the yield rate and Faradaic efficiency (FE) of acetate by the PtCu NF/C could reach $8.49 \mu\text{L}/(\text{h mg}_{\text{Pt}})$ and 98.2% at the given potential, higher than

that of PtCu ND/C [$4.40 \mu\text{L}/(\text{h mg}_{\text{Pt}})$ and 48.6%] and Pt/C [$0.30 \mu\text{L}/(\text{h mg}_{\text{Pt}})$ and 5.75%] (Figure S16e,f), demonstrating that the combination of Cu, high-index facets, and multi-channel structures is beneficial to improve the yield and selectivity of acetate. In addition, as displayed in Figure S9d, EIS results suggest that PtCu NF/C has a smaller semicircle radius among the two different catalysts, indicating its higher charge-transfer rate and faster catalytic kinetics.

To reveal the superiority by PtCu NF/C for the coupled HER and EOR, the potential differences between HER and EOR at 10 mA cm^{-2} were evaluated (Figure 3a). PtCu NF/C requires a lower potential difference of 0.58 V in coupled reactions than the commercial Pt/C (0.76 V), suggesting the application potential of PtCu NF/C as an effective bifunctional catalyst for electrochemical hydrogen generation coupled with ethanol oxidation. By comparing the LSV curves of PtCu NF/C and the commercial Pt/C in 1.0 M KOH with and without ethanol, both of them need smaller potentials in 1.0 M KOH + 0.5 M ethanol than the corresponding OER (Figure S17),

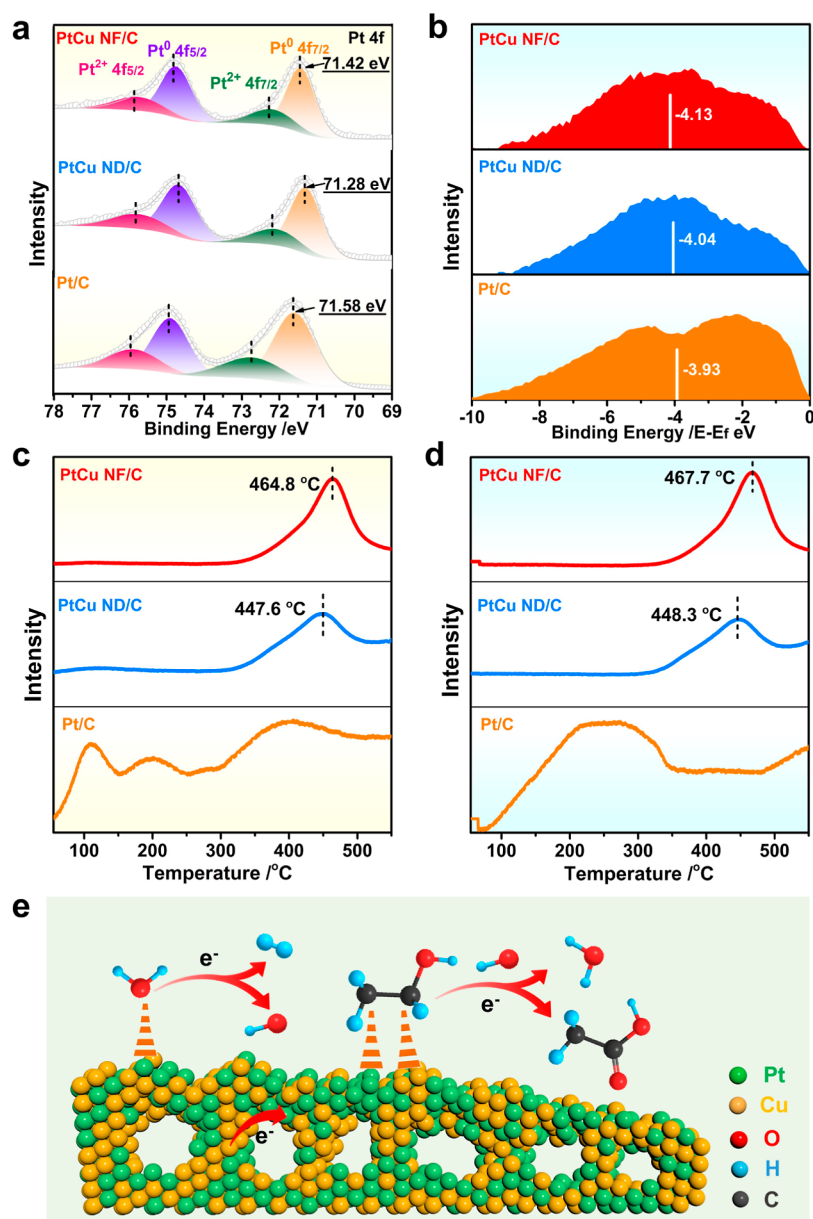


Figure 4. (a) Pt 4f spectra and (b) valence-band spectra, (c) CH₃CH₂OH-TPD profiles, and (d) H₂O-TPD profiles of PtCu NF/C, PtCu ND/C, and the commercial Pt/C. (e) Schematic illustration of the mechanism for EOR and HER on PtCu NF/C.

showing that the ethanol electrochemical reforming is an efficient approach for hydrogen production. Furthermore, the coupled HER/EOR performances of the two catalysts were further evaluated in a two-electrode system (Figure 3b). The PtCu NF/C requires a voltage of 0.58 V for the coupled HER/EOR at 10 mA cm⁻², overmatching the 0.75 V needed for the commercial Pt/C (Figure 3c,d). In addition, they are both much lower than those needed for the coupled HER/OER (1.88 and 1.92 V, respectively) (Figure S18). These results show that energy-saving hydrogen production can be achieved by combining HER with favorable EOR. During the test, a large number of bubbles generated and can be observed in the cathode, indicating that a large amount of hydrogen was produced (Figure S19). In addition, the FE of H₂ by PtCu NF/C was as high as 92% at 0.6 V (Figure S20). Moreover, *I*-*t* tests were conducted on PtCu NF/C and the commercial Pt/C at 0.62 V (Figure 3e). After the durability test, PtCu NF/C could largely maintain their 3D morphologies with only a small

Cu loss as confirmed by SEM-EDS (Figure S21a,b). Besides that, Pt and Cu could exist stably without significant change in valence after the durability test (Figure S21c,d), while there are obvious agglomerations for the commercial Pt/C (Figure S22).

To further verify the advantages of PtCu NF/C in the electrochemical reforming of ethanol for hydrogen production, the performance of initial PtCu ND/C and PtCu NCF/C for the coupled HER and EOR in both three-electrode and two-electrode systems was also evaluated. First, the potential difference needed for PtCu ND/C is 0.66 V at 10 mA cm⁻² in coupled reactions (Figure S23a), which is larger than that of the PtCu NF/C. Then, the potential difference at 10 mA cm⁻² of coupled HER/EOR in the three-electrode system (0.90 V) (Figure S23b) and the voltage difference in the two-electrode system (1.28 V) (Figure S23c) for PtCu ND/C is still smaller than 0.94 and 1.30 V for PtCu NF/C. In addition, the voltage needed for coupled HER/EOR at 10 mA cm⁻² by PtCu NF/C (0.58 V) is also much lower than that of the PtCu ND/C (0.66

V). As for PtCu NCF/C, a potential difference of 0.61 V at 10 mA cm⁻² is required in coupled reactions (Figure S24a). In addition, the potential differences of 0.92 and 1.27 V are coupled HER/EOR in three-electrode system and two-electrode system (Figure S24b,c). Furthermore, the voltage needed for the coupled HER/EOR by PtCu NCF/C is 0.60 V (Figure S24c). The results mentioned above confirm the crucial role of synergistic effect between surface and structure regulation in PtCu NF/C for electrochemical reforming of ethanol to produce H₂.

Furthermore, methanol, ethylene glycol, and glycerol were used to replace ethanol as anode electrolytes in a similar two-electrode cell to study the versatility of PtCu NF/C for coupled HER with other alcohols to achieve energy-saving hydrogen production (Figure S25). For HER/methanol oxidation reaction (Figure S25a,b), HER/ethylene glycol oxidation reaction (Figure S25c,d), and HER/glycerol oxidation reaction (Figure S25e,f), PtCu NF/C exhibits the lowest voltage among the three different catalysts, suggesting that the high-index facets and the multi-channels of PtCu NF/C possess a high catalytic activity. In addition, compared with electrochemical water splitting, the voltages needed by the PtCu NF/C in electro-oxidation of various alcohols at 10 mA cm⁻² are obviously reduced, indicating the excellent electrochemical performance of PtCu NF/C (Table S4). Therefore, PtCu NF/C with the synergistic effect between high-index facets and the multi-channels is a kind of the promising and efficient catalyst for coupled HER with other alcohols to achieve energy-saving hydrogen production.

In order to figure out the unique catalytic activity of PtCu NF/C, we first used XPS to analyze their electronic structure (Figures 4, S26 and S27). It can be seen in Figure 4a that there are two peaks belonging to the states of Pt 4f_{7/2} and Pt 4f_{5/2} in the Pt 4f spectrum of PtCu NF/C, and each peak can be further divided into two double peaks related to Pt⁰ and Pt²⁺, respectively.^{34,35} As for Cu, Cu 2p_{3/2} and Cu 2p_{1/2} can be also divided into two doublets of Cu⁰ and Cu²⁺.^{36,37} Compared with PtCu ND/C, the Pt 4f_{7/2} peak of the PtCu NF/C slightly shifts to the higher value (Figure 4a), while the Cu 2p binding energy in PtCu NF/C shifts to the lower binding energy (Figure S27), indicating that the electron transfer and electronic structure changes of Pt and Cu occurred after the dealloying process. Besides, the change in the electronic structure is also likely associated with the abundant high-index facets on the PtCu NF/C surface, which would provide more possibilities for the adsorption, activation, and dissociation of intermediates, resulting in enhanced catalytic performance.

The valence-band spectra of PtCu NF/C, PtCu ND/C, and the commercial Pt/C indicated that the d-band center of PtCu NF/C shifts downward to PtCu ND/C and the commercial Pt/C (Figure 4b), revealing that PtCu NF/C with high-index facets and multi-channel structure has the strongest adsorption energy for reaction intermediate among the three different catalysts, leading to the enhanced HER and EOR activities.³⁸ Such enhanced adsorption can be also confirmed from the CH₃CH₂OH temperature-programmed desorption (CH₃CH₂OH-TPD) and H₂O-TPD. As shown in Figure 4c,d, the PtCu NF/C (464.8 and 467.7 °C) exhibited higher CH₃CH₂OH and H₂O adsorption temperatures than PtCu ND/C (447.6 and 448.3 °C) and the commercial Pt/C (~100 and ~400 °C, ~200 °C), suggesting that high-index facets and multi-channel structure improved CH₃CH₂OH and H₂O adsorption for PtCu NF/C, resulting in a stronger bonding

strength of CH₃CH₂OH and H₂O than PtCu ND/C and the commercial Pt/C. Above all, we believe that the strong interaction between Pt and Cu, high-index facets, as well as the 3D open structure of PtCu NF/C synergistically erupt into the outstanding performance of EOR/HER with excellent activity and selectivity (Figure 4e).

CONCLUSIONS

In conclusion, we designed a class of unique PtCu NF/C with high-index facets and multi-channels as an efficient bifunctional electrocatalyst for HER and EOR. The PtCu NF/C can be also used as both anodic and cathodic catalysts for the two-electrode system, which can couple HER and EOR under mild conditions to achieve energy-saving hydrogen production and achieve high-value anode products. Furthermore, the results show that PtCu NF/C requires only 0.58 V in the coupled HER/EOR to equal the amount of hydrogen produced by water splitting at 1.88 V. The FE of H₂ produced at the cathode is close to 92%, while the conversion efficiency of ethanol into acetate at the anode is up to 98.2%. Mechanistic investigations reveal that the combination of open 3D structure, Cu introduction, and high-index facets endows the PtCu NF/C with enhanced adsorption capacity for ethanol and H₂O, as well as dissociation capacity for C–H bonds of ethanol. Moreover, PtCu NF/C can also realize energy-saving hydrogen production by oxidizing other alcohols (methanol, ethylene glycol, and glycerol) to replace OER. Meanwhile, high-value anode products could be obtained. Our work not only provides an emerging and economical approach to facilitate the energy-saving hydrogen production but also proposes new ideas for the design of efficient catalysts for more catalytic reactions.

EXPERIMENTAL SECTION

Materials. Platinum(II) acetylacetonate (Pt(acac)₂, 97%) was bought from Sigma-Aldrich. Copper chloride dihydrate (CuCl₂·2H₂O, AR), acetic acid (C₂H₄O₂, ≥99.8%), D(+)-glucose anhydrous (C₆H₁₂O₆, reagent grade), methanol (CH₃OH, AR), ethanol (CH₃CH₂OH, AR), ethylene glycol (C₂H₆O₂, AR), glycerol (C₃H₈O₃, AR), and cyclohexane (C₆H₁₂, AR) were received from Sinopharm Chemical Reagent Co. Ltd. (Shanghai, China). Hexadecyltrimethylammonium bromide (C₁₉H₄₂BrN, CTAB, 99%) and oleylamine (C₁₈H₃₇N, OAm, 68–70%) were obtained from J&K Scientific Ltd. (Beijing, China). The water (18 MΩ cm⁻²) used was obtained from the ultra-pure purification system.

Electrocatalyst Preparation. For PtCu ND, Pt(acac)₂ (10 mg), CuCl₂·2H₂O (6.5 mg), CTAB (36.5 mg), C₆H₁₂O₆ (60 mg), and OAm (5 mL) were added into a glass vial (30 mL) and then ultrasonicated for 30 min to obtain a homogeneous solution. It was heated to 180 °C for 5 h in an oil bath. Finally, the PtCu ND was further obtained by centrifugation and washed with ethanol/cyclohexane mixture.

PtCu NF/C was prepared via etching the PtCu ND/C by acetic acid. First, PtCu ND was supported on Vulcan XC-72R carbon by sonication and further washed with ethanol and dried in a vacuum oven at 60 °C. The PtCu ND/C was redispersed in 5 mL of deionized water to obtain a homogeneous dispersion, and then, 1 mL of acetic acid was added into the mixture. Finally, the mixture was heated to 60 °C for 5 h under stirring to obtain the PtCu NF/C. The

preparation for PtCu NCF/C was similar to that of PtCu NF/C, except that acetic acid was changed to nitric acid.

Characterizations. TEM images were obtained using a JEM-2100plus operating at 200 kV. High-magnification TEM and STEM images were acquired on a Tecnai F20 TEM from FEI at 200 kV. PXRD was conducted by a BRUKER AXS GMBH D8 diffractometer with a Cu $K\alpha$ X-ray source ($\lambda = 1.542 \text{ \AA}$). SEM-EDS was carried out with a HITACHI S-4800 cold field emission SEM. XPS analysis was conducted with an Axis supra (Kratos Analytical Ltd). The ICP data were received from an ICP-OES (Varian 710-ES).

Electrochemical Measurements. Electrochemical measurements were carried out in a three-electrode cell, while the reference and counter electrodes are saturated calomel electrode (SCE) and carbon rod, respectively. $1.0 \text{ mg}_{\text{Pt}} \text{ mL}^{-1}$ of catalyst was obtained by dispersing in isopropanol and nafion (5 wt %). $2.0 \mu\text{L}$ of PtCu NF/C and PtCu ND/C suspension were dropped on the glassy carbon electrode (GCE) to prepare the working electrode. The SCE was calibrated to RHE before electrochemical measurements. The TOF of H_2 was calculated to evaluate their intrinsic activity of per active sites of the commercial Pt/C, PtCu ND/C, and PtCu NF/C. The underpotential deposition of H (Q_{H}) on Pt was used to quantify their corresponding active sites with the following equation: $n = Q_{\text{H}}/F$. Then, the TOF was calculated by $\text{TOF} = I/2Fn$. Among them, I is the current based on LSV, F stands for the Faraday constant, n stands for the number of active sites. $1/2$ represents that two electrons are needed to obtain one H_2 molecule.

HER was conducted in 1.0 M KOH and 0.5 M H_2SO_4 . The LSV curves for HER were recorded at 5 mV s^{-1} without iR-corrected. The chronoamperometric test for HER in 1.0 M KOH was performed at 10 mA cm^{-2} . EOR was conducted in 1.0 M KOH + 0.5 M $\text{C}_2\text{H}_5\text{OH}$ during -0.86 – $0.35 \text{ V}_{\text{SCE}}$ at 50 mV s^{-1} . A two-electrode cell was prepared for the coupled HER/EOR (1.0 M KOH + 0.5 M $\text{C}_2\text{H}_5\text{OH}$ and 1.0 M KOH in anode and cathode cells) in the H-type cell separated by the membrane of Nafion 211. In addition, anode and cathode cells are both 1.0 M KOH for overall water splitting. The GCE loaded with catalysts ($15.3 \mu\text{g}_{\text{Pt}} \text{ cm}^{-2}$) was used as the anodic and cathodic catalysts. The coupled HER/alcohol oxidation reactions were tested in 1.0 M KOH + 0.5 M $\text{CH}_3\text{OH}/\text{C}_2\text{H}_6\text{O}_2/\text{C}_3\text{H}_8\text{O}_3$ at 50 mV s^{-1} . The FE could be calculated by $\text{FE} = eF \times n/Q$, where F is the Faraday constant, Q is the total charge, e is the number of electrons transferred for the different products, and n is the total amount of the different products.

■ ASSOCIATED CONTENT

SI Supporting Information

The Supporting Information is available free of charge at <https://pubs.acs.org/doi/10.1021/acscatal.2c03022>.

Structural and compositional characterizations of PtCu ND and PtCu ND/C; formation process of PtCu NF/C; TEM image of the commercial Pt/C; electrochemical test data; structural and compositional characterizations of PtCu NCF/C; HER performance of PtCu NCF/C; EOR performance of PtCu ND/C and PtCu NCF/C; ^1H NMR analysis, yield rates, and FE; polarization curves; photograph of the two-electrode cell; GC; characterization after the durability test, polarization curves of PtCu ND/C and PtCu NCF/C; HER/MOR, HER/EGOR, and HER/GOR; XPS analysis; ICP data;

and performance comparison of HER, EOR, and coupled HER/alcohol oxidation reaction (Tables S2–S4) (PDF)

■ AUTHOR INFORMATION

Corresponding Authors

Nan Zhang – Key Laboratory of Synthetic and Biological Colloids, Ministry of Education, School of Chemical and Material Engineering, International Joint Research Laboratory for Nano Energy Composites, Jiangnan University, Wuxi 214122, China; orcid.org/0000-0002-2177-0544; Email: nzhang@jiangnan.edu.cn

Tianxi Liu – Key Laboratory of Synthetic and Biological Colloids, Ministry of Education, School of Chemical and Material Engineering, International Joint Research Laboratory for Nano Energy Composites, Jiangnan University, Wuxi 214122, China; orcid.org/0000-0002-5592-7386; Email: txliu@jiangnan.edu.cn

Authors

Hui Fu – Key Laboratory of Synthetic and Biological Colloids, Ministry of Education, School of Chemical and Material Engineering, International Joint Research Laboratory for Nano Energy Composites, Jiangnan University, Wuxi 214122, China

Feili Lai – Department of Chemistry, KU Leuven, Leuven 3001, Belgium; orcid.org/0000-0002-4945-0737

Longsheng Zhang – Key Laboratory of Synthetic and Biological Colloids, Ministry of Education, School of Chemical and Material Engineering, International Joint Research Laboratory for Nano Energy Composites, Jiangnan University, Wuxi 214122, China

Suli Chen – Key Laboratory of Synthetic and Biological Colloids, Ministry of Education, School of Chemical and Material Engineering, International Joint Research Laboratory for Nano Energy Composites, Jiangnan University, Wuxi 214122, China

Hanjun Li – Key Laboratory of Synthetic and Biological Colloids, Ministry of Education, School of Chemical and Material Engineering, International Joint Research Laboratory for Nano Energy Composites, Jiangnan University, Wuxi 214122, China

Kezhu Jiang – School of Materials Science and Engineering, Hebei University of Technology, Tianjin 300401, China

Ting Zhu – National Laboratory of Solid-State Microstructures/School of Electronics Science and Engineering/Collaborative Innovation Center of Advanced Microstructures, Nanjing University, Nanjing 210093, China

Fangping Xu – Key Laboratory of Synthetic and Biological Colloids, Ministry of Education, School of Chemical and Material Engineering, International Joint Research Laboratory for Nano Energy Composites, Jiangnan University, Wuxi 214122, China

Complete contact information is available at: <https://pubs.acs.org/doi/10.1021/acscatal.2c03022>

Notes

The authors declare no competing financial interest.

■ ACKNOWLEDGMENTS

This work was financially supported by the National Natural Science Foundation of China (NSFC) (22105087 and

52161135302) and the Natural Science Foundation of Jiangsu Province (BK20210446). The authors thank the Central Laboratory, School of Chemical and Material Engineering, Jiangnan University.

REFERENCES

- (1) Lubitz, W.; Tumas, W. Hydrogen: An overview. *Chem. Rev.* **2007**, *107*, 3900–3903.
- (2) Wang, M.; Chen, L.; Sun, L. Recent progress in electrochemical hydrogen production with earth-abundant metal complexes as catalysts. *Energy Environ. Sci.* **2012**, *5*, 6763–6778.
- (3) Nocera, D. G. The artificial leaf. *Acc. Chem. Res.* **2012**, *45*, 767–776.
- (4) Jia, Y.; Zhang, L.; Gao, G.; Chen, H.; Wang, B.; Zhou, J.; Soo, M. T.; Hong, M.; Yan, X.; Qian, G.; Zou, J.; Du, A.; Yao, X. A heterostructure coupling of exfoliated Ni–Fe hydroxide nanosheet and defective graphene as a bifunctional electrocatalyst for overall water splitting. *Adv. Mater.* **2017**, *29*, 1700017.
- (5) Peng, W.; Jin, J.; Yang, S.; Shen, Z.; Wang, H.; Zhang, J.; Li, G. Hollow Co₉S₈ spheres-derived polyhedrons uniformly anchored on N, S-doped graphene for efficient oxygen electrocatalysts. *Compos. Commun.* **2021**, *23*, 100587.
- (6) You, B.; Sun, Y. Innovative strategies for electrocatalytic water splitting. *Acc. Chem. Res.* **2018**, *51*, 1571–1580.
- (7) Qian, Q.; Zhang, J.; Li, J.; Li, Y.; Jin, X.; Zhu, Y.; Liu, Y.; Li, Z.; El-Harairy, A.; Xiao, C.; Zhang, G.; Xie, Y. Artificial heterointerfaces achieve delicate reaction kinetics towards hydrogen evolution and hydrazine oxidation catalysis. *Angew. Chem., Int. Ed.* **2021**, *60*, 5984–5993.
- (8) Luo, J.; Im, J. H.; Mayer, M. T.; Schreier, M.; Nazeeruddin, M. K.; Park, N. G.; Tilley, S. D.; Fan, H. J.; Grätzel, M. Water photolysis at 12.3% efficiency via perovskite photovoltaics and earth-abundant catalysts. *Science* **2014**, *345*, 1593–1596.
- (9) Zhao, X.; Dai, L.; Qin, Q.; Pei, F.; Hu, C.; Zheng, N. Self-supported 3D PdCu alloy nanosheets as a bifunctional catalyst for electrochemical reforming of ethanol. *Small* **2017**, *13*, 1602970.
- (10) Li, M.; Duanmu, K.; Wan, C.; Cheng, T.; Zhang, L.; Dai, S.; Chen, W.; Zhao, Z.; Li, P.; Fei, H.; Zhu, Y.; Yu, R.; Luo, J.; Zang, K.; Lin, Z.; Ding, M.; Huang, J.; Sun, H.; Guo, J.; Pan, X.; Goddard, W. A.; Sautet, P.; Huang, Y.; Duan, X. Single-atom tailoring of platinum nanocatalysts for high-performance multifunctional electrocatalysis. *Nat. Catal.* **2019**, *2*, 495–503.
- (11) Kwon, Y.; Kim, Y.; Hong, J. W.; Whang, Y.; Kim, S.; Wi, D. H.; Byon, H. R.; Han, S. W. One-pot production of ceria nanosheet-supported PtNi alloy nanodendrites with high catalytic performance toward methanol oxidation and oxygen reduction. *J. Mater. Chem. A* **2020**, *8*, 25842–25849.
- (12) Kim, T.; Roy, S. B.; Moon, S.; Yoo, S.; Choi, H.; Parale, V. G.; Kim, Y.; Lee, J.; Jun, S. C.; Kang, K.; Chun, S. H.; Kanamori, K.; Park, H. H. Highly dispersed Pt clusters on F-doped tin(IV) oxide aerogel matrix: An ultra-robust hybrid catalyst for enhanced hydrogen evolution. *ACS Nano* **2022**, *16*, 1625–1638.
- (13) Jeong, S.; Mai, H. D.; Nam, K. H.; Park, C. M.; Jeon, K. J. Self-healing graphene-templated platinum–nickel oxide heterostructures for overall water splitting. *ACS Nano* **2022**, *16*, 930–938.
- (14) Dai, C.; Yang, Y.; Zhao, Z.; Fisher, A.; Liu, Z.; Cheng, D. From mixed to three-layer core/shell PtCu nanoparticles: Ligand-induced surface segregation to enhance electrocatalytic activity. *Nanoscale* **2017**, *9*, 8945–8951.
- (15) Tian, X.; Zhao, X.; Su, Y. Q.; Wang, L.; Wang, H.; Dang, D.; Chi, B.; Liu, H.; Hensen, E. J. M.; Lou, X. W.; Xia, B. Y. Engineering bunched Pt–Ni alloy nanocages for efficient oxygen reduction in practical fuel cells. *Science* **2019**, *366*, 850–856.
- (16) Bai, S.; Wang, L.; Li, Z.; Xiong, Y. Facet-engineered surface and interface design of photocatalytic materials. *Adv. Sci.* **2017**, *4*, 1600216.
- (17) Xie, C.; Niu, Z.; Kim, D.; Li, M.; Yang, P. Surface and interface control in nanoparticle catalysis. *Chem. Rev.* **2020**, *120*, 1184–1249.
- (18) Zhang, N.; Shao, Q.; Xiao, X.; Huang, X. Advanced catalysts derived from composition-segregated platinum–nickel nanostructures: New opportunities and challenges. *Adv. Funct. Mater.* **2019**, *29*, 1808161.
- (19) Gong, M.; Xiao, D.; Deng, Z.; Zhang, R.; Xia, W.; Zhao, T.; Liu, X.; Shen, T.; Hu, Y.; Lu, Y.; Zhao, X.; Xin, H.; Wang, D. Structure evolution of PtCu nanoframes from disordered to ordered for the oxygen reduction reaction. *Appl. Catal., B* **2021**, *282*, 119617.
- (20) Hu, J.; Cao, L.; Wang, Z.; Liu, J.; Zhang, J.; Cao, Y.; Lu, Z.; Cheng, H. Hollow high-entropy metal organic framework derived nanocomposite as efficient electrocatalyst for oxygen reduction reaction. *Compos. Commun.* **2021**, *27*, 100866.
- (21) Bu, L.; Ding, J.; Guo, S.; Zhang, X.; Su, D.; Zhu, X.; Yao, J.; Guo, J.; Lu, G.; Huang, X. A general method for multimetallic platinum alloy nanowires as highly active and stable oxygen reduction catalysts. *Adv. Mater.* **2015**, *27*, 7204–7212.
- (22) Zhang, Z.; Liu, G.; Cui, X.; Chen, B.; Zhu, Y.; Gong, Y.; Saleem, F.; Xi, S.; Du, Y.; Borgna, A.; Lai, Z.; Zhang, Q.; Li, B.; Zong, Y.; Han, Y.; Gu, L.; Zhang, H. Crystal phase and architecture engineering of lotus-thalamus-shaped Pt–Ni anisotropic superstructures for highly efficient electrochemical hydrogen evolution. *Adv. Mater.* **2018**, *30*, 1801741.
- (23) Wang, Z. Y.; Zhang, B.; Liu, S.; Li, G. R.; Yan, T.; Gao, X. P. Nickel–platinum alloy nanocrystallites with high-index facets as highly effective core catalyst for lithium–sulfur batteries. *Adv. Funct. Mater.* **2022**, *32*, 2200893.
- (24) Kwon, T.; Jun, M.; Kim, H. Y.; Oh, A.; Park, J.; Baik, H.; Joo, S. H.; Lee, K. Vertex-reinforced PtCuCo ternary nanoframes as efficient and stable electrocatalysts for the oxygen reduction reaction and the methanol oxidation reaction. *Adv. Funct. Mater.* **2018**, *28*, 1706440.
- (25) Wang, Z.; Wu, X.; Liu, J.; Zhang, D.; Zhao, H.; Zhang, X.; Qin, Y.; Nie, N.; Wang, D.; Lai, J.; Wang, L. Ordered vacancies on the body-centered cubic PdCu nanocatalysts. *Nano Lett.* **2021**, *21*, 9580–9586.
- (26) Zhang, N.; Li, L.; Wang, J.; Hu, Z.; Shao, Q.; Xiao, X.; Huang, X. Surface-regulated rhodium–antimony nanorods for nitrogen fixation. *Angew. Chem., Int. Ed.* **2020**, *59*, 8066–8071.
- (27) Niu, Z.; Becknell, N.; Yu, Y.; Kim, D.; Chen, C.; Kornienko, N.; Somorjai, G. A.; Yang, P. Anisotropic phase segregation and migration of Pt in nanocrystals en route to nanoframe catalysts. *Nat. Mater.* **2016**, *15*, 1188–1194.
- (28) Anantharaj, S.; Noda, S. Layered 2D PtX₂ (X = S, Se, Te) for the electrocatalytic HER in comparison with Mo/WX₂ and Pt/C: Are we missing the bigger picture? *Energy Environ. Sci.* **2022**, *15*, 1461–1478.
- (29) Pang, Q. Q.; Niu, Z. L.; Yi, S. S.; Zhang, S.; Liu, Z. Y.; Yue, X. Z. Hydrogen-etched bifunctional sulfur-defect-rich ReS₂/CC electrocatalyst for highly efficient HER and OER. *Small* **2020**, *16*, 2003007.
- (30) Du, R.; Jin, W.; Hübner, R.; Zhou, L.; Hu, Y.; Eychmüller, A. Engineering multimetallic aerogels for pH-universal HER and ORR electrocatalysis. *Adv. Energy Mater.* **2020**, *10*, 1903857.
- (31) Nguyen, D.; Luyen Doan, T. L.; Prabhakaran, S.; Tran, D. T.; Kim, D. H.; Lee, J. H.; Kim, N. H. Hierarchical Co and Nb dual-doped MoS₂ nanosheets shelled micro-TiO₂ hollow spheres as effective multifunctional electrocatalysts for HER, OER, and ORR. *Nano Energy* **2021**, *82*, 105750.
- (32) Liu, C.; Pan, G.; Liang, N.; Hong, S.; Ma, J.; Liu, Y. Ir single atom catalyst loaded on amorphous carbon materials with high HER activity. *Adv. Sci.* **2022**, *9*, 2105392.
- (33) Wang, K.; Huang, D.; Guan, Y.; Liu, F.; He, J.; Ding, Y. Fine-tuning the electronic structure of dealloyed PtCu nanowires for efficient methanol oxidation reaction. *ACS Catal.* **2021**, *11*, 14428–14438.
- (34) Li, H. H.; Fu, Q. Q.; Xu, L.; Ma, S. Y.; Zheng, Y. R.; Liu, X. J.; Yu, S. H. Highly crystalline PtCu nanotubes with three dimensional molecular accessible and restructured surface for efficient catalysis. *Energy Environ. Sci.* **2017**, *10*, 1751–1756.
- (35) Hong, Y. R.; Dutta, S.; Jang, S. W.; Ngame Okello, O. F.; Im, H.; Choi, S.-Y.; Han, J. W.; Lee, I. S. Crystal Facet-Manipulated 2D Pt

Nanodendrites to Achieve an Intimate Heterointerface for Hydrogen Evolution Reactions. *J. Am. Chem. Soc.* **2022**, *144*, 9033–9043.

(36) Zhang, C.; Wang, P.; Li, W.; Zhang, Z.; Zhu, J.; Pu, Z.; Zhao, Y.; Mu, S. MOF-assisted synthesis of octahedral carbon-supported PtCu nanoalloy catalysts for an efficient hydrogen evolution reaction. *J. Mater. Chem. A* **2020**, *8*, 19348–19356.

(37) Zheng, Y.; Zhang, J.; Ma, Z.; Zhang, G.; Zhang, H.; Fu, X.; Ma, Y.; Liu, F.; Liu, M.; Huang, H. Seeded growth of gold–copper janus nanostructures as a tandem catalyst for efficient electroreduction of CO₂ to C₂₊ products. *Small* **2022**, *18*, 2201695.

(38) Song, Z.; Zhu, Y. N.; Liu, H.; Banis, M. N.; Zhang, L.; Li, J.; Doyle-Davis, K.; Li, R.; Sham, T. K.; Yang, L.; Young, A.; Botton, G. A.; Liu, L. M.; Sun, X. Engineering the low coordinated Pt single atom to achieve the superior electrocatalytic performance toward oxygen reduction. *Small* **2020**, *16*, 2003096.

Recommended by ACS

Intermetallic PtCu Nanoframes as Efficient Oxygen Reduction Electrocatalysts

Ho Young Kim, Sang Hoon Joo, *et al.*

SEPTEMBER 14, 2020
NANO LETTERS

READ 

Cu₂O-Derived PtCu Nanoalloy toward Energy-Efficient Hydrogen Production via Hydrazine Electrolysis under Large Current Density

Shangmeng Ge, Xijun Liu, *et al.*

AUGUST 09, 2022
ACS APPLIED ENERGY MATERIALS

READ 

External and Internal Interface-Controlled Trimetallic PtCuNi Nanoframes with High Defect Density for Enhanced Electrooxidation of Liquid Fuels

Daowei Gao, Guozhu Chen, *et al.*

JANUARY 24, 2020
CHEMISTRY OF MATERIALS

READ 

Ultrathin and Porous 2D PtPdCu Nanoalloys as High-Performance Multifunctional Electrocatalysts for Various Alcohol Oxidation Reactions

Jinwu Hu, Zhiqing Cui, *et al.*

JUNE 08, 2022
INORGANIC CHEMISTRY

READ 

Get More Suggestions >